

Optimization of broadband optical response of multilayer nanospheres

Wenjun Qiu,¹ Brendan G. DeLacy,² Steven G. Johnson,³
John D. Joannopoulos,¹ and Marin Soljačić^{1*}

¹Department of Physics, Massachusetts Institute of Technology
77 Massachusetts Avenue, Cambridge Massachusetts 02139, USA

²Edgewood Chemical Biological Center, Research & Technology Directorate
5183 Blackhawk Rd., Aberdeen Proving Ground, MD 21010, USA

³Department of Mathematics, Massachusetts Institute of Technology
77 Massachusetts Avenue, Cambridge Massachusetts 02139, USA

*[soljacic@mit.edu](mailto:solja@mit.edu)

Abstract: We propose an optimization-based theoretical approach to tailor the optical response of silver/silica multilayer nanospheres over the visible spectrum. We show that the structure that provides the largest cross-section per volume/mass, averaged over a wide frequency range, is the silver coated silica sphere. We also show how properly chosen mixture of several species of different nanospheres can have an even larger minimal cross-section per volume/mass over the entire visible spectrum.

© 2012 Optical Society of America

OCIS codes: (290.5825) Scattering theory; (290.2200) Extinction.

References and links

1. Y. Pu, R. Grange, C.-L. Hsieh, and D. Psaltis, "Nonlinear optical properties of core-shell nanocavities for enhanced second-harmonic generation," *Phys. Rev. Lett.* **104**, 207402 (2010).
2. X. Huang, S. Neretina, and M. A. El-Sayed, "Gold nanorods: From synthesis and properties to biological and biomedical applications," *Adv. Mater.* **21**, 4880–4910 (2009).
3. C. Noguez, "Surface plasmons on metal nanoparticles: the influence of shape and physical environment," *J. Phys. Chem. C* **111**, 3806–3819 (2007).
4. S. Alyones, C. Bruce, and A. Buin, "Numerical methods for solving the problem of electromagnetic scattering by a thin finite conducting wire," *IEEE Trans. Antennas Propag.* **55**, 1856–1861 (2007).
5. C. W. Bruce and S. Alyones, "Extinction efficiencies for metallic fibers in the infrared," *Appl. Opt.* **48**, 5095–5098 (2009).
6. P. K. Jain, K. S. Lee, I. H. El-Sayed, and M. A. El-Sayed, "Calculated absorption and scattering properties of gold nanoparticles of different size, shape, and composition: Applications in biological imaging and biomedicine," *J. Phys. Chem. B* **110**, 7238–7248 (2006).
7. J. Zhu, J. Li, and J. Zhao, "Tuning the wavelength drift between resonance light absorption and scattering of plasmonic nanoparticle," *Appl. Phys. Lett.* **99**, 101901 (2011).
8. C. E. Román-Velázquez and C. Noguez, "Designing the plasmonic response of shell nanoparticles: Spectral representation," *J. Chem. Phys.* **134**, 044116 (2011).
9. S. Oldenburg, R. Averitt, S. Westcott, and N. Halas, "Nanoengineering of optical resonances," *Chem. Phys. Lett.* **288**, 243–247 (1998).
10. E. Prodan and P. Nordlander, "Structural tunability of the plasmon resonances in metallic nanoshells," *Nano Lett.* **3**, 543–547 (2003).
11. E. Prodan, C. Radloff, N. J. Halas, and P. Nordlander, "A hybridization model for the plasmon response of complex nanostructures," *Science* **302**, 419–422 (2003).
12. R. Bardhan, N. K. Grady, T. Ali, and N. J. Halas, "Metallic nanoshells with semiconductor cores: Optical characteristics modified by core medium properties," *ACS Nano* **4**, 6169–6179 (2010).
13. R. Bardhan, S. Mukherjee, N. A. Mirin, S. D. Levit, P. Nordlander, and N. J. Halas, "Nanosphere-in-a-nanoshell: A simple nanomaterial," *J. Phys. Chem. C* **114**, 7378–7383 (2010).

14. R. E. Hamam, A. Karalis, J. D. Joannopoulos, and M. Soljačić, "Coupled-mode theory for general free-space resonant scattering of waves," *Phys. Rev. A* **75**, 053801 (2007).
15. Z. Ruan and S. Fan, "Superscattering of light from subwavelength nanostructures," *Phys. Rev. Lett.* **105**, 013901 (2010).
16. Z. Ruan and S. Fan, "Temporal coupled-mode theory for fano resonance in light scattering by a single obstacle," *J. Phys. Chem. C* **114**, 7324–7329 (2010).
17. Z. Ruan and S. Fan, "Design of subwavelength superscattering nanospheres," *Appl. Phys. Lett.* **98**, 043101 (2011).
18. H. C. van de Hulst, *Light Scattering by Small Particles* (Dover, 1981).
19. C. Bohren and D. Huffman, *Absorption and Scattering of Light by Small Particles* (John Wiley & Sons, 1983).
20. E. D. Palik, *Handbook of Optical Constants of Solids* (Academic Press, New York, 1985).
21. S. G. Johnson, "The nlopt nonlinear optimization package, <http://ab-initio.mit.edu/nlopt>," .
22. S. Kucherenko and Y. Sytsko, "Application of deterministic low-discrepancy sequences in global optimization," *Comput. Optim. Appl.* **30**, 297–318 (2005).
23. M. J. D. Powell, "The bobyqa algorithm for bound constrained optimization without derivatives," Tech. rep., Department of Applied Mathematics and Theoretical Physics, Cambridge England (2009).
24. N. T. Fofang, T.-H. Park, O. Neumann, N. A. Mirin, P. Nordlander, and N. J. Halas, "Plexcitonic nanoparticles: Plasmonexciton coupling in nanoshell j-aggregate complexes," *Nano Lett.* **8**, 3481–3487 (2008).
25. A. Yoshida and N. Kometani, "Effect of the interaction between molecular exciton and localized surface plasmon on the spectroscopic properties of silver nanoparticles coated with cyanine dye j-aggregates," *J. Chem. Phys. C* **114**, 2867–2872 (2010).
26. V. S. Lebedev, A. S. Medvedev, D. N. Vasil'ev, D. A. Chubich, and A. G. Vitukhnovsky, "Optical properties of noble-metal nanoparticles coated with a dye j-aggregate monolayer," *Quantum Electron.* **40**, 246–248 (2010).

1. Introduction

Nanoparticles with strong optical response, characterized by scattering, absorption and total cross-sections, have wide applications in biomedical imaging, photothermal therapy, and optical obscuration [1–3]. Different applications require different optical response properties. For instance, real-time biomedical imaging is based on large scattering cross-sections, while photothermal therapy requires nanoparticles with large absorption cross-sections and small scattering cross-sections. For obscuration applications [4, 5], the ideal nanoparticle should typically have large total cross-sections over the whole visible spectrum while keeping the volume or mass of nanoparticles as small as possible. The diversity and complexity of these requirements necessitate an engineering approach of nanoparticle design.

Previous studies on the optical response of nanoparticles are mainly based on parametric approach [6–8], which works well for simple structures. However, when the structure becomes complicated and the number of design parameters increases, optimization becomes the preferable approach because it can efficiently explore the whole parameter space. Furthermore, because the optimization objective function can be an arbitrary transformation of the frequency-dependent cross-sections, this approach is very powerful in tailoring the broadband optical response of nanoparticles. For example, some applications may require that the optical resonance has both a strong peak value and a wide bandwidth. This can be achieved by maximizing the average cross-section over the bandwidth of interest. For obscuration applications, we want the total cross-section to be consistently large over the whole visible spectrum. This is equivalent to maximizing the minimal cross-section over this spectrum. In this paper, we will use an optimization tool to tailor the optical response of multilayer nanospheres over wide frequency range of interest.

Before we start, we need to select the material system. Nanoparticles composed of metal and dielectric materials support surface plasmons on the metal/dielectric interfaces and can strongly interact with light in the visible range [9–13]. At resonance, the cross-sections of these nanoparticles are much larger than their physical cross-sections, which makes them superscatterers and super-absorbers [14–17]. Furthermore, the plasmon resonance frequency can be tuned by varying the physical structure of the nanoparticles. In order to be able to tailor the optical response of nanoparticles over a wide frequency range, we choose the metal/dielectric

material system. For concreteness, we will focus on the silver/silica material system.

In this article, we first formulate the Transfer Matrix Method to calculate the optical response of multilayer nanospheres. After briefly reviewing the optical response of bilayer silver/silica nanospheres, we proceed to optimize the average cross-section of various silver/silica multilayer nanospheres. Our optimization results show that the structure with the maximal average cross-section is the bilayer silver/silica structure with silver as the shell. Finally, we investigate using a mixture of several species of bilayer nanospheres to enhance the minimal cross-sections over the entire visible range.

2. Calculation of optical response via transfer matrix method

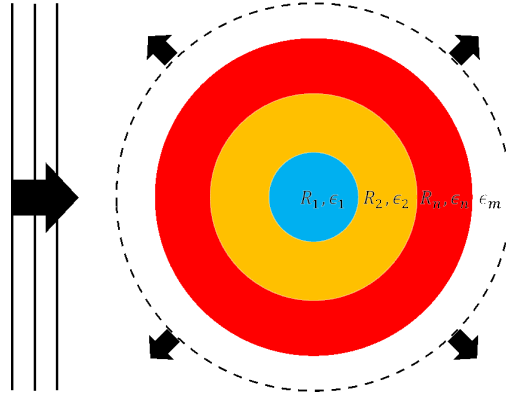


Fig. 1. Schematic of an n layer nanosphere embedded in infinite dielectric medium. The outer radius and dielectric function of individual layers are $(R_i, \epsilon_i), i = 1, 2, \dots, n$. The dielectric function of the medium is ϵ_m . The solid lines represent an incident plane wave which contains incoming and outgoing waves. The dashed line represents the scattered wave which only contains outgoing wave.

We start by formulating the Transfer Matrix Method for multilayer nanosphere [18, 19]. Consider a multilayer nanosphere shown in Fig. 1. Because of the spherical symmetry, the fields at a given incident frequency can be decomposed into two orthogonal polarizations: transverse electric (TE) and transverse magnetic (TM). For TE polarization, the electric fields can be written as $\mathbf{E}_{TE} = \nabla \times \mathbf{r}\phi_{TE}$. For TM polarization, the magnetic fields can be written as $\mathbf{H}_{TM} = \nabla \times \mathbf{r}\phi_{TM}$. The scalar potential ϕ_{TE} and ϕ_{TM} satisfy the scalar Helmholtz equation $\nabla^2 \phi + k^2 \phi = 0$ where $k^2 = \omega^2 \epsilon(\mathbf{r})$. Due to the spherical symmetry, ϕ can be decomposed into a discrete set of spherical modes: $\phi_{lm} = R_l(r)P_l^m(\cos \theta) \exp(im\varphi)$ with $l = 0, 1, 2, \dots$ and $m = -l, \dots, l$. Since $\epsilon(\mathbf{r})$ is a constant ϵ_i inside the i^{th} shell, $R_l(r)$ is a linear combination of the first and second kind spherical Bessel functions within the individual shells:

$$R_l(r)|_i = A_i j_l(k_i r) + B_i y_l(k_i r) \quad (1)$$

The coefficients (A_i, B_i) of adjacent shells are linked by the transfer matrix of the interface:

$$\begin{bmatrix} A_{i+1} \\ B_{i+1} \end{bmatrix} = M_{i+1,i} \begin{bmatrix} A_i \\ B_i \end{bmatrix} \quad (2)$$

The matrix element is determined by the boundary condition satisfied by $R_l(r)$, which comes from the continuity of the tangent components of \mathbf{E} and \mathbf{H} across the boundary. For TE po-

larization, $rR_l(r)$ and $(rR_l(r))'$ are continuous across the boundary. By writing the continuity conditions in matrix form, we get:

$$M_{i+1,i} = \begin{bmatrix} j_l(k_{i+1}R_i) & y_l(k_{i+1}R_i) \\ j'_l(k_{i+1}R_i)k_{i+1}R_i + j_l(k_{i+1}R_i) & y'_l(k_{i+1}R_i)k_{i+1}R_i + y_l(k_{i+1}R_i) \end{bmatrix}^{-1} \times \begin{bmatrix} j_l(k_iR_i) & y_l(k_iR_i) \\ j'_l(k_iR_i)k_iR_i + j_l(k_iR_i) & y'_l(k_iR_i)k_iR_i + y_l(k_iR_i) \end{bmatrix} \quad (3)$$

For TM polarization, $rR_l(r)$ and $(\epsilon^{-1}rR_l(r))'$ are continuous across the boundary. By writing the continuity conditions in matrix form, we get:

$$M_{i+1,i} = \begin{bmatrix} j_l(k_{i+1}R_i) & y_l(k_{i+1}R_i) \\ j'_l(k_{i+1}R_i)k_{i+1}R_i + j_l(k_{i+1}R_i) & y'_l(k_{i+1}R_i)k_{i+1}R_i + y_l(k_{i+1}R_i) \end{bmatrix}^{-1} \times \begin{bmatrix} j_l(k_iR_i) & y_l(k_iR_i) \\ \frac{\epsilon_{i+1}}{\epsilon_i}(j'_l(k_iR_i)k_iR_i + j_l(k_iR_i)) & \frac{\epsilon_{i+1}}{\epsilon_i}(y'_l(k_iR_i)k_iR_i + y_l(k_iR_i)) \end{bmatrix} \quad (4)$$

The transfer matrix of the whole system can be calculated by cascading the transfer matrices of individual interfaces.

$$\begin{bmatrix} A_{n+1} \\ B_{n+1} \end{bmatrix} = M_{n+1,n}M_{n,n-1}\dots M_{3,2}M_{2,1} \begin{bmatrix} A_1 \\ B_1 \end{bmatrix} = M \begin{bmatrix} A_1 \\ B_1 \end{bmatrix} \quad (5)$$

Since the second kind of Bessel function is singular at the origin, we can set $A_1 = 1$ and $B_1 = 0$. So the coefficients of Bessel functions in the surrounding medium are directly given by the transfer matrix element, $A_{n+1} = M_{11}$ and $B_{n+1} = M_{21}$. Within the surrounding medium, it is convenient to write the radical function as a linear combination of the spherical Hankel functions:

$$R_l(r)|_{n+1} = C_{n+1}h_l^1(k_{n+1}r) + D_{n+1}h_l^2(k_{n+1}r) \quad (6)$$

Taking the convention that the fields vary in time as $e^{-i\omega t}$, $h_l^1(k_{n+1}r)$ and $h_l^2(k_{n+1}r)$ correspond to outgoing and incoming waves respectively. The reflection coefficient of the whole system is given by

$$r_l = \frac{C_{n+1}}{D_{n+1}} = \frac{M_{11} - iM_{21}}{M_{11} + iM_{21}} \quad (7)$$

The reflection coefficient as a function of frequency determines the optical response of the nanoparticle under all possible illumination conditions. Specifically, when the nanoparticle is illuminated by a linearly polarized plane wave, the incident field can be decomposed into both TE and TM channels (l, m) with $l = 1, 2, \dots$ and $m = -1, 1$. For each channel, the incident field contains both incoming and outgoing waves carrying the same power [14–17]

$$P_{l,m=\pm 1} = \frac{\lambda^2}{16\pi} (2l+1)I_0 \quad (8)$$

where I_0 is the incident intensity, and λ is the wavelength in the surrounding medium. The scattered field is a purely outgoing wave characterized by the scattering coefficient S_l which is related to the reflection coefficient through $S_l = (r_l - 1)/2$. The scattered and absorbed power

in this channel is given by:

$$P_{l,m=\pm 1}^{sca} = \frac{\lambda^2}{16\pi} (2l+1) I_0 |1 - r_l|^2 \quad (9)$$

$$P_{l,m=\pm 1}^{abs} = \frac{\lambda^2}{16\pi} (2l+1) I_0 (1 - |r_l|^2) \quad (10)$$

By summing over the contribution from all channels of TE and TM polarization, we get the scattering and absorption cross-sections:

$$\sigma_{sca} = \sum_{\sigma} \sum_{l=1}^{\infty} \frac{\lambda^2}{8\pi} (2l+1) |1 - r_{\sigma,l}|^2 \quad (11)$$

$$\sigma_{abs} = \sum_{\sigma} \sum_{l=1}^{\infty} \frac{\lambda^2}{8\pi} (2l+1) (1 - |r_{\sigma,l}|^2) \quad (12)$$

where σ is TE or TM. The total cross-section is the sum of the scattering and absorption cross-sections. $\sigma_{tot} = \sigma_{sca} + \sigma_{abs}$.

3. Optical response of silver/silica bilayer nanospheres

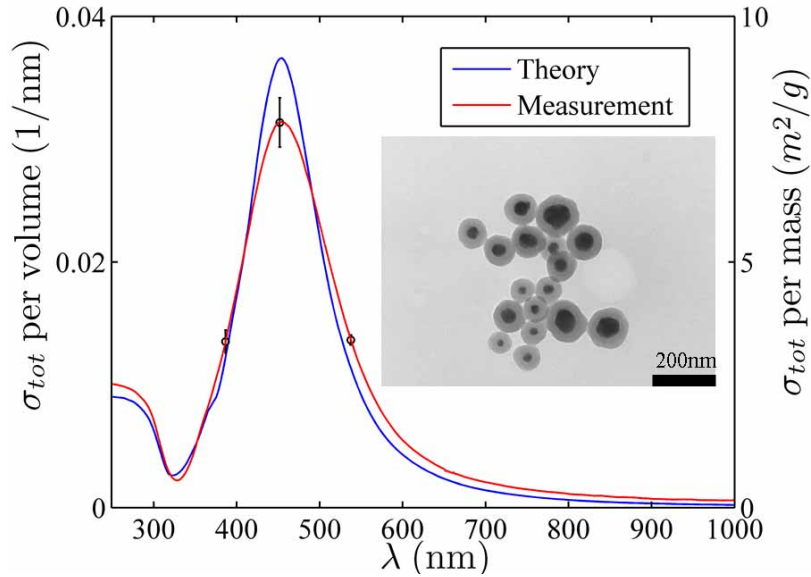


Fig. 2. The total cross-section of silica coated silver spheres suspended in ethanol. The cross-section is normalized by volume (the left axis) and mass (the right axis). The insert is a TEM image of the fabricated nanoparticles. The radius of the silver core has a distribution with mean 26.3nm and standard deviation 9.3nm. The thickness of the silica shell is around 25.3nm. The red line is the measured total cross-section. The black bar represents the standard deviations from eight transmission measurement on eight samples. The blue line is the Transfer Matrix calculation of the total cross-section with the radius of the silver core sampled from the measured distribution and the thickness of the silica shell fixed at 25.3nm. The dielectric function of ethanol is taken as $\epsilon_m = 1.85$.

In this section, we analyze the optical response of silver/silica bilayer nanospheres as the building elements of multilayer structures. For silver, the complex dielectric function as a function of frequency is generated by linearly interpolating the experimental data [20]. For simplicity, the size dependence of Ag's dielectric function is not taken into account. For silica, the dielectric function is taken as a constant $\epsilon = 2.1$. There are two configurations of silver/silica bilayer nanoparticle depending on the core material.

First, we consider silica coated silver spheres. Colloidal suspensions of such nanoparticles were obtained from Nanocomposix (Nanocomposix Inc., San Diego, CA). Figure 2 shows the measured and calculated total cross-sections of the fabricated nanoparticles. The calculation agrees quite well with the measurement. The total cross-section peaks around 455nm. This peak comes from the $l = 1$ surface plasmon mode at the silver/silica boundary. The peak wavelength only varies slightly when the inner and outer radius change. For instance, consider a silica coated silver sphere suspended in air. Fixing the outer radius at 50nm, the peak wavelength varies from 410nm to 415nm when the inner radius varies from 5nm to 45nm. Fixing the aspect ratio R_1/R_2 at 0.8, the peak wavelength varies from 390nm to 480nm when the outer radius varies from 25nm to 75nm.

In contrast, the surface plasmon resonance of the reverse configuration has great tunability over the visible range [9–13]. Consider a silver coated silica sphere suspended in air. Fixing the outer radius at 50nm, the peak wavelength varies from 405nm to 720nm when the inner radius varies from 5nm to 45nm. Besides the peak wavelength, the relative strength of scattering and absorption cross-sections in the total cross-section also vary. For $[R_1, R_2] = [5\text{nm}, 50\text{nm}]$, the absorption cross-section accounts for 25% of the total cross-section at resonance. For $[R_1, R_2] = [45\text{nm}, 50\text{nm}]$, this percentage rises to 60%. The tunability of the resonance wavelength and the tunability of the total cross-section composition makes silver coated silica sphere a good candidate for achieving broadband optical response.

4. Optimization of average cross-sections over wide frequency range

The optical response of silver/silica bilayer nanosphere indicates that increasing the number of metal/dielectric interfaces can provide additional tunability in the optical response. Using this insight, we aim to design silver/silica multilayer nanosphere with a large average cross-section over wide frequency range. The figure of merit (FOM) is the scattering, absorption, and total cross-section averaged over the target frequency range, normalized by volume or mass.

$$FOM = \frac{1}{\omega_{max} - \omega_{min}} \int_{\omega_{min}}^{\omega_{max}} \sigma_{normalized} d\omega \quad (13)$$

For concreteness, we take 400-600nm and 600-800nm as the target frequency range of interest. The structure under consideration is a multilayer nanosphere with alternating silver and silica layers (six layers in total). The design parameters are the thicknesses of individual layers. The lower bounds of the thicknesses are set to be zero. The upper bound of the allowed thickness is set to be a large value ($1\mu\text{m}$). Therefore, this general structure includes structures with fewer layers (one through five layers) as boundary points.

We performed the optimization using numerical optimization package NLOPT [21]. Since this problem is nonconvex, there are many local optima. To find the global optima in the design parameter space, we used Multi-Level-Single-Linkage (MLSL) algorithm. This algorithm performs a sequence of local optimization from random points by a clustering heuristic that helps it to avoid repeated searches of the same optima [22]. The local optimization algorithm used here is BOBYQA [23]. This algorithm performs derivative-free bound-constrained optimization using an iteratively constructed quadratic approximation of the objective function.

Figure 3 summarizes the optimization results. In all cases, the optimal structure returned by

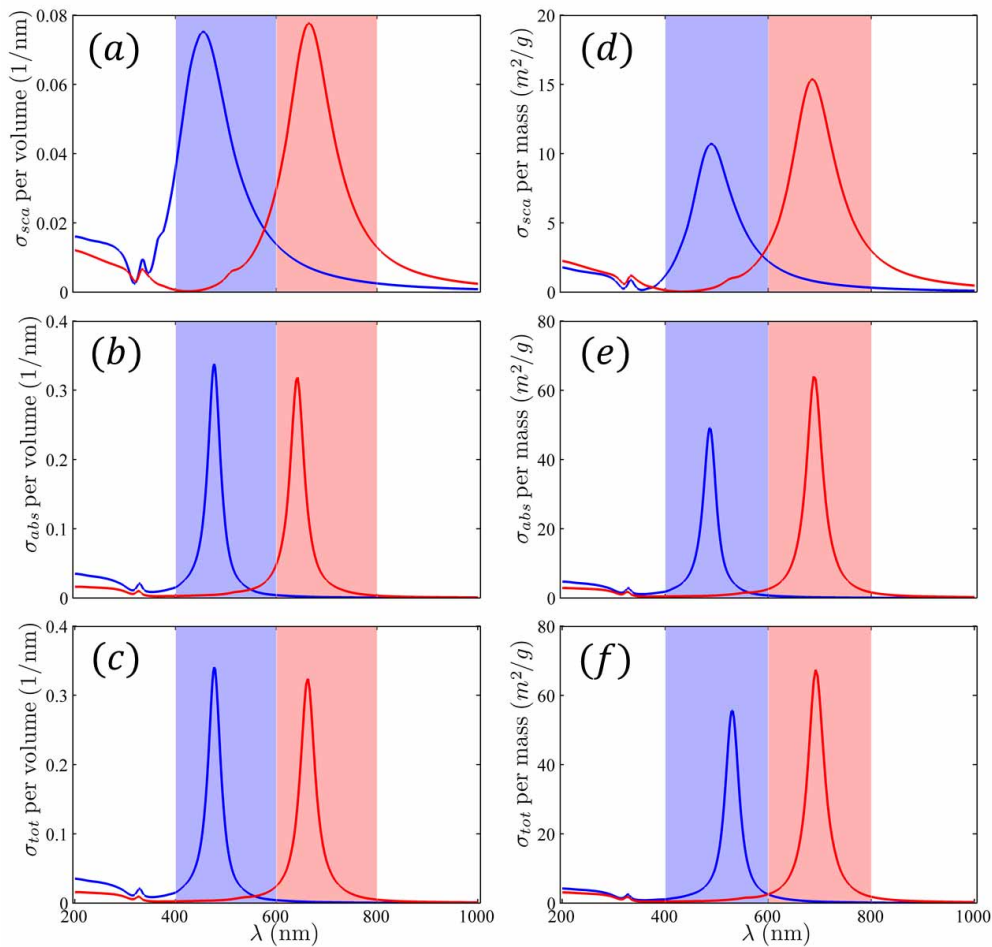


Fig. 3. Optimization of average cross-sections over wide frequency range. The structure under consideration is a silver/silica multilayer nanosphere. The optimal structure found by the optimization engine is always silver coated silica sphere. For all subfigures, blue (red) lines show the optimized average cross-sections over the blue (red) shaded frequency range. (a)(b)(c) correspond to scattering, absorption and total cross-sections per volume respectively. (d)(e)(f) correspond to scattering, absorption and total cross-sections per mass respectively. The radius of the silica cores and the thickness of silver shells exhibiting the cross-sections shown above are given in Table 1.

the optimization engine is always a silver coated silica sphere. Although multilayer structures can offer greater tunability of the optical response, bilayer structures already maximize the average cross-section over wide frequency range. From Table 1, we can see that nanospheres with an outer radius around 70nm have the largest normalized average scattering cross-section. The wavelength of the scattering peak can be further tuned by varying the aspect ratio. For absorption cross-sections, our optimization engine found many local optima with approximately equal FOM's. These local optima have the same aspect ratio, and the thickness of the silver layer varies from zero to several nanometers. This can be explained by the quasi-static approximation. The absorption cross-section of a nanoparticle can be written as $\sigma_{abs}(\omega) = \omega \text{Im}[\alpha(\omega)]$,

where $\alpha(\omega)$ is the polarizability [24–26]. When the nanoparticle diameter is much smaller than the wavelength, the quasi-static approximation is valid, under which the polarizability is proportional to the volume of the nanoparticle with the proportionality coefficient dependent on frequency and aspect ratio [24]. Therefore, the normalized absorption cross-section averaged over a frequency range is only determined by the aspect ratio and independent of the nanoparticle diameter as long as the nanoparticle diameter is much smaller than the wavelength. In Table 2, the thickness of the silver layer is set to be ≥ 2 nm. Nanospheres with thinner silver layers have approximately the same normalized average absorption cross-section but are difficult to fabricate. The structures that give the largest average scattering and absorption cross-sections are quite different. Since the FOM of the absorption cross-section is about twice as large as the FOM of the scattering cross-section, the structure that gives the largest average total cross-section is essentially identical to the structure providing the largest average absorption cross-section. The structures given in Table 1 are super-scatters and super-absorbers. For instance, the structure with $[R, T] = [60.40\text{nm}, 8.68\text{nm}]$ has an average scattering cross-section of $8.65\text{m}^2/\text{g}$ over 600-800nm, while its physical cross-section is only $2.07\text{m}^2/\text{g}$. The structure with $[R, T] = [18.09\text{nm}, 2.00\text{nm}]$ provides an average total cross-section of $17.52\text{m}^2/\text{g}$ over 600-800nm, which means that only 1g of such nanoparticles, when fully dispersed, can obscure an area as large as 17.52m^2 .

Table 1. Optimization of average cross-sections

Normalized by volume				
cross-section	range (nm)	silica (nm)	silver (nm)	FOM (1/nm)
σ_{sca}	400-600	31.25	26.65	0.0486
	600-800	60.32	9.65	0.0464
σ_{abs}	400-600	6.07	2.00	0.0767
	600-800	14.80	2.00	0.0817
σ_{tot}	400-600	6.09	2.00	0.0773
	600-800	16.12	2.00	0.0846

Normalized by mass				
cross-section	range (nm)	silica (nm)	silver (nm)	FOM (m^2/g)
σ_{sca}	400-600	38.53	17.88	5.64
	600-800	60.40	8.68	8.65
σ_{abs}	400-600	6.54	2.00	10.87
	600-800	17.89	2.00	16.71
σ_{tot}	400-600	8.71	2.00	10.93
	600-800	18.09	2.00	17.52

5. Optimization of the minimal cross-sections over wide frequency range

In this section, we aim to design nanoparticles with consistently large cross-sections over a wide frequency range. This is equivalent to maximizing the minimal cross-section over the target frequency range. From the previous section, we see that silver coated silica spheres have strong surface plasmon resonances, and the peaks of their resonances are highly tunable. Therefore, we expect that a mixture of several species of silver coated silica spheres with different resonance frequencies can effectively cover a wide frequency range.

This intuition can be formalized by optimization language. We take the target wavelength range to be 400-800nm. The FOM is the minimal cross-section over this range, normalized by

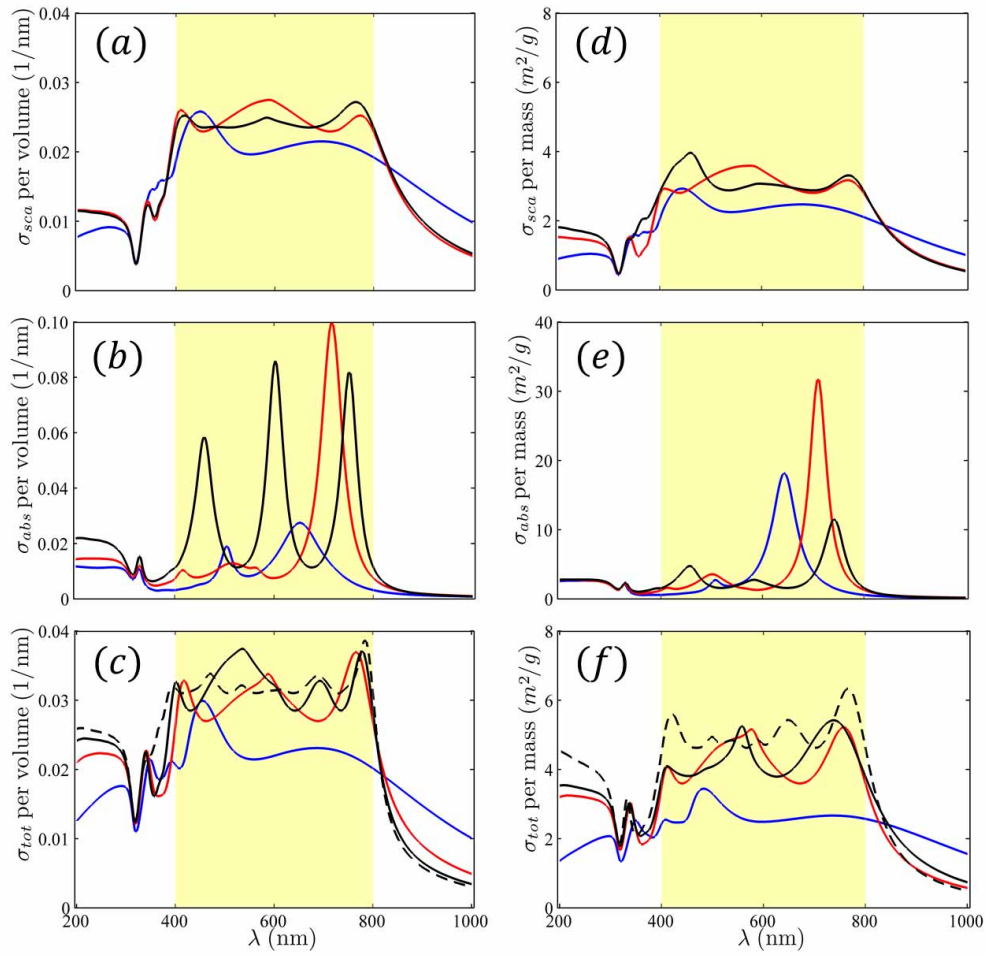


Fig. 4. Optimization of minimal cross-sections over a wide frequency range. The structure under consideration is a mixture of several species of silver coated silica spheres. The target frequency range is shaded in yellow. For all subfigures, blue, red, black lines corresponds to one, two, and three species of nanospheres. The black dashed lines in (c) and (f) correspond to ten species of nanospheres. (a)(b)(c) correspond to scattering, absorption, and total cross-sections per volume respectively. (d)(e)(f) correspond to scattering, absorption and total cross-sections per mass respectively. The radius of the silica cores and the thickness of silver shells corresponding to these cross-sections are given in Table 2.

either volume or mass.

$$FOM = \min_{\omega} \sigma_{normalized} \quad (14)$$

The structure under consideration is a mixture of N species of silver coated silica spheres where $N = 1, 2, 3, \dots$. The design parameters are the size parameters of individual species and relative weights (i.e. proportions) of each species in the mixture. The weights represent the relative

weights in volume (mass) when the normalization is over volume (mass).

$$\sigma_{normalized} = \sum_{i=1}^N w_i \sigma_{i,normalized} \quad (15)$$

When the size parameters of individual species are fixed, the problem of finding the optimal weights turns out to be a Linear Programming (LP) program. Therefore, we employed a two-level optimization structure. In the lower level, we used a standard LP solver to find out the optimal weights given the current size parameters. The resulting FOM as a function of size parameters is further optimized in the upper level with the same nonlinear method we used in the previous section. This separation into linear and nonlinear parts of the original optimization problem reduces the dimension of the parameter space and helps MLSL algorithm to find the global optimal in less iterations.

Figure 4 summarizes the results. We can see that the optimization engine tries to build a plateau over the target range to maximize the minimal cross-section. For scattering cross-sections, it is relatively easy to build such a plateau since the scattering peaks have wide bandwidth. When there is only one species (the blue lines in Fig. 4(a)(d)), the nanoparticle has a large size so that its $l = 1$ resonance can cover the large wavelength region and its $l = 2$ resonance can cover the small wavelength region. When the number of species increases, the new species try to cover the dips in the original scattering spectra with their resonant peaks. On the other hand, it is relatively difficult to build an absorption plateau because absorption peaks have narrow bandwidth. The FOM of the scattering cross-section is about twice as large as that of the absorption cross-section. The total cross-section can be enhanced significantly (35% for volume normalization and 46% for mass normalization) when N increases from 1 to 2. The enhancement when N increases from 2 to 3 is only moderate. The benefit of adding more species gradually saturates.

6. Concluding remarks

In this article, we used optimization tools to tailor the optical response of silver/silica multilayer spheres. We show that the structure that gives the largest average cross-section over wide frequency range is the bilayer structure with a silver shell. We also show that using several species of nanoparticles can significantly enhance the minimal cross-section over the whole visible range although this enhancement saturates when the number of species increase. Because the FOM can be an arbitrary function of the frequency dependent cross-sections, the optimization approach described here can be used to design nanoparticles with more complicated optical response. We are investigating efficient numerical methods of calculating and optimizing the optical response of non-spherical geometries as future directions.

This research was funded by the Department of the Army Basic Research Program and sponsored by the Edgewood Chemical Biological Center. Support was also provided by the U.S. Army Research Office under contract W911NF-07-D-004.

Table 2. Optimization of minimal cross-sections

Normalized by volume

cross-section	# of species	silica (nm)	silver (nm)	weights (%)	FOM (1/nm)
σ_{sca}	1	68.09	55.44	100	0.0192
		52.54	44.21	82.8	
	3	73.41	7.63	17.2	0.0235
		52.85	47.27	74.4	
		75.61	8.31	20.8	
		35.55	23.21	4.8	
σ_{abs}	1	60.14	10.00	100	0.0032
		37.03	4.00	57.5	
	3	44.02	15.99	42.5	0.0114
		22.95	10.26	37.4	
		26.08	4.39	34.3	
		21.96	2.00	28.3	
σ_{tot}	1	80.15	41.87	100	0.0201
		59.96	34.12	82.8	
	3	61.96	6.29	17.2	0.0270
		50.21	32.98	75.2	
		52.97	4.90	14.4	
		55.76	7.32	10.4	
	10	0.0310

Normalized by mass

cross-section	# of species	silica (nm)	silver (nm)	weights (%)	FOM (m ² /g)
σ_{sca}	1	67.95	52.38	100	2.10
		52.77	38.70	87.4	
	3	75.72	8.17	12.6	2.80
		76.71	21.93	46.1	
		21.96	34.54	43.2	
		70.45	7.31	10.7	
σ_{abs}	1	42.80	6.55	100	0.58
		20.56	2.15	51.3	
	3	37.16	13.61	48.7	1.31
		27.43	14.22	36.9	
		49.06	11.02	34.9	
		36.66	3.66	28.2	
σ_{tot}	1	92.95	39.04	100	2.46
		55.54	29.60	83.5	
	3	67.77	7.39	16.5	3.59
		53.36	29.01	60.1	
		79.49	10.25	31.1	
		24.64	25.04	8.8	
	10	4.62